RANDOM IS ALL YOU NEED: RANDOM NOISE INJECTION ON FEATURE STATISTICS FOR GENERALIZABLE DEEP IMAGE DENOISING

Anonymous authors
Paper under double-blind review

ABSTRACT

Recent advancements in generalizable deep image denoising have catalyzed the development of robust noise-handling models. The current state-of-the-art, Masked Training (MT), constructs a masked SwinIR model which is trained exclusively on Gaussian noise (σ=15) but can achieve commendable denoising performance across various noise types (*i.e.* speckle noise, poisson noise). However, this method, while focusing on content reconstruction, often produces over-smoothed images and poses challenges in mask ratio optimization, complicating its integration with other methodologies. In response, this paper introduces RNINet, a novel architecture built on a streamlined encoder-decoder framework to enhance both efficiency and overall performance. Initially, we train a pure RNINet (only simple encoder-decoder) on individual noise types, observing that feature statistics such as mean and variance shift in response to different noise conditions. Leveraging these insights, we incorporate a noise injection block that injects random noise into feature statistics within our framework, significantly improving generalization across unseen noise types. Our framework not only simplifies the architectural complexity found in MT but also delivers superior performance. Comprehensive experimental evaluations demonstrate that our method outperforms MT in various unseen noise conditions in terms of denoising effectiveness and computational efficiency (lower MACs and GPU memory usage), achieving up to 10 times faster inference speeds and underscoring it's capability for large scale deployments.

1 INTRODUCTION

Image denoising is a critical area of research in low-level image processing aimed at recovering clean images from noisy counterparts. The rapid advancements in deep learning have inspired numerous studies proposing specialized image denoising networks. These networks, typically trained on pre-defined noise distributions, show remarkable performance in noise removal. However, their generalization to other noise types is limited, restricting their application in real-world scenarios where noise distributions often vary from those in the training phase.

In the current research trend on the image denoising task, most existing works (*i.e.* SwinIR (Liang et al., 2021), Restormer (Zamir et al., 2022)) train and evaluate models on images corrupted with Gaussian noise, which limits their performance to this specific noise distribution. To address this limitation, some methods (Zhang et al., 2017) assume an unknown noise level for a particular noise type, while others (Brooks et al., 2019b; Wei et al., 2020) attempt to improve the performance in real-world scenarios by synthesizing or collecting training data closer to the target noise or directly performing unsupervised training on the target noise (Chen et al., 2018; Yuan et al., 2018). Despite these efforts, recent work by Chen et al. (Chen et al., 2023) argues that none of these methods substantially improve the generalization performance of denoising networks, and they still struggle when the noise distribution is mismatched (Abdelhamed et al., 2018b). In response, they propose masked training and construct a masked SwinIR model which learns the reconstruction of image textures and structures rather than overfitting to a specific noise type, their model is trained on Gaussian noise $\sigma = 15$ but can generalize well to other different unseen noise types. Nevertheless, we notice that despite the enhanced performances, their model also introduces unwanted side-effects that tends to over-smooth image contents, leading to the loss of high-frequency details and a drop in PSNR (refer to Fig. 1).

The generalization challenge in deep denoising continues to be a significant hurdle for broader applicability.

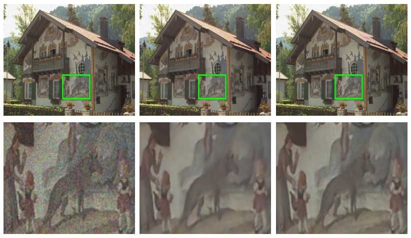
Noisy Image MT (29.87 dB) Ours (31.67 dB)

Figure 1: The side-effects of MT (Chen et al., 2023) on image quality: Over-smoothing of content results in a decrease in PSNR. In contrast, our method preserves more details while removing noise, thereby achieving higher PSNR.

In this paper, we present RNINet, a novel architecture built on a streamlined encoder-decoder framework to enhance both efficiency and overall performance for generalizable deep image denoising. Initially, we train a pure RNINet (only simple encoder-decoder) on individual noise types and observe that feature statistics, such as mean and variance, shift in response to different noise conditions (refer to Fig. 2). Some recent studies (Liu et al., 2021; 2023; Chen et al., 2023) have conduct generalization analysis experiment based on feature statistics distribution, but none of them conduct manipulations directly on the learned feature statistics. Leveraging these insights, we incorporate noise injection blocks within RNINet to inject random noise on feature statistics, thereby creating noised features that influence the model's learning. While feature statistics can contain domain-specific information (Huang & Belongie, 2017; Li et al., 2021), this noise injection manipulation allows the noised feature statistics to represent potential unseen noise domains, significantly enhancing the model's generalization capabilities. The main contributions of this work are summarized as follows:

- We present RNINet, a novel architecture that utilizes a streamlined encoder-decoder framework to both enhance efficiency and improve the performance of generalizable deep image denoising. This approach simplifies the architectural complexity typically found in existing generalizable denoising methods, facilitating broader application to real-world deployment environments.
- We introduce a noise injection block that injects random noise into feature statistics, aimed at potential unseen noise domains. This development significantly enhances generalization capabilities, distinguishing our approach from existing research that primarily focuses on generalization analysis without direct operational interventions.
- Comprehensive experiments demonstrate that RNINet surpasses the performance of the state-of-the-art method MT in various unseen noise conditions, delivering superior denoising effectiveness and computational efficiency (lower MACs and GPU memory usage), achieving up to 10 times faster inference speeds and underscoring it's capability for large scale deployments.

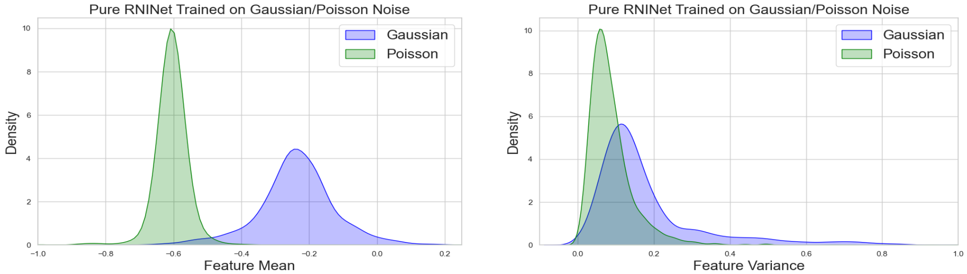

Figure 2: Impact of training with different noise on feature statistics. We investigate the shifts in mean and variance by initially training a pure RNINet (only simple encoder-decoder) with Gaussian and Poisson noise. The feature statistics exhibit markedly different distributions for each noise type.

2 RELATED WORK

2.1 IMAGE DENOISING

Image denoising techniques predominantly fall into two categories: traditional model-based methods and data-driven deep learning approaches. Traditional methods (Buades et al., 2005; Dabov et al., 2007; Elad & Aharon, 2006; Gu et al., 2014; Mairal et al., 2009) generally rely on modeling image priors to recover content from images affected by noise, demonstrating a certain level of flexibility and generalization capability (Abdelhamed et al., 2018b) across various noise types. However, these methods often struggle to reconstruct fine image details and achieve high PSNR. In contrast, data-driven deep learning models have achieved remarkable denoising performance. CNN models (Zhang et al., 2017; 2022; Lefkimmiatis, 2018; 2017; Mao et al., 2016; Divakar & Venkatesh Babu, 2017; Jia et al., 2019; Zhang et al., 2018) were once the mainstream in denoising models, offering substantial performance improvements over traditional methods. The advent of Vision Transformers (Dosovitskiy et al., 2020), which treat pixels as tokens and leverage self-attention to parse token interactions, has marked a significant paradigm shift. Variants based on Vision Transformers (Zamir et al., 2022; Liang et al., 2021; Zhao et al., 2023; Zhang et al., 2023a; Wang et al., 2022; Chen et al., 2021; 2022b) have largely supplanted CNN models as the mainstream solution due to their enhanced capability to capture global dependencies. Despite these advancements, a prevalent issue is the training of models on noise patterns identical to those encountered during testing, where the primary performance metric becomes the network's capacity to overfit training noise.

2.2 GENERALIZATION PROBLEM

The generalization dilemma in low-level vision tasks, such as image denoising, often emerges when there is a discrepancy between training and testing degradations. Conventionally, models are trained on Gaussian noise, a practice misaligned with the predominantly non-Gaussian noise encountered in real-world scenarios, leading to performance degradation. To address this, solutions have diverged into two primary methodologies: one seeks to simulate real-world noise more closely during training (Brooks et al., 2019b; Wei et al., 2020; Chen et al., 2018; Guo et al., 2019; Plotz & Roth, 2017; Krull et al., 2019; Abdelhamed et al., 2018b), while the other develops 'blind' denoising models assuming that the noise level is unknown or training on a large amount of noise types (Krull et al., 2019; Yue et al., 2019; Zhang et al., 2023b; 2017). Recent work by Chen et al. (Chen et al., 2023) has pointed out that these efforts do not sufficiently delve into the generalization shortfalls; these methods still fail to generalize to noise types not represented in the training dataset. Some studies (Liu et al., 2021; 2023) have attempted to analyze the reasons behind poor generalization capabilities of super-resolution models and have identified that conventional training methods tend to make models overfit specific degradation type to achieve higher PSNR. Building on these insights, Chen et al. (Chen et al., 2023) introduced masked training and constructed a masked SwinIR (Liang et al., 2021), designed to focus on content reconstruction rather than overfitting specific noise types. While their approach achieved commendable results, it also introduced some unwanted side-effects: the image content tends to be over-smoothed, leading to a loss of high-frequency details and a drop in PSNR performance. Most recently, Cheng et al. (Cheng et al., 2024) enhanced generalization performance by incorporating a pretrained CLIP model. However, because the CLIP model has been exposed to prior information from billions of images containing diverse noise types, their method is categorized into another independent track and often excluded from direct comparisons with benchmark methods that were solely trained with Gaussian noise, to ensure fairness.

2.3 FEATURE STATISTICS IN NEURAL NETWORKS

Feature statistics (*i.e.* mean and variance) are commonly utilized in the analysis of various neural networks, with research (Huang & Belongie, 2017; Li et al., 2021) indicating that they can capture informative characteristics of specific domains (e.g., color, texture, and contrast). In scenarios involving out-of-distribution data, feature statistics often demonstrate inconsistencies with those of the training domain due to differing domain characteristics (Wang et al., 2019; Gao et al., 2021), while some normalization methods (Ioffe & Szegedy, 2015; Li et al., 2022) can also improve model performance by manipulating feature statistics. Recent studies in the field of low-level vision have also explored model generalization capabilities with feature statistics. For instance, (Liu et al., 2023) proposed a metric based on feature statistics to assess the generalization ability of super-resolution models, while (Liu et al., 2021) introduced the CHI evaluation score following dimensionality reduction and clustering based on feature statistics. Subsequently, MT (Chen et al., 2023) utilized the metric from (Liu et al., 2021) to validate the generalization performance of their generalizable denoising models. However, these studies typically treat feature statistics as deterministic values obtained from the features and rely solely on statistical analysis of these values to validate the generalization capability and efficacy of their methods. In contrast, our approach provide a novel perspective that injects random noise tensors to alter feature statistics, thereby enhancing the generalization capability of our denoising models.

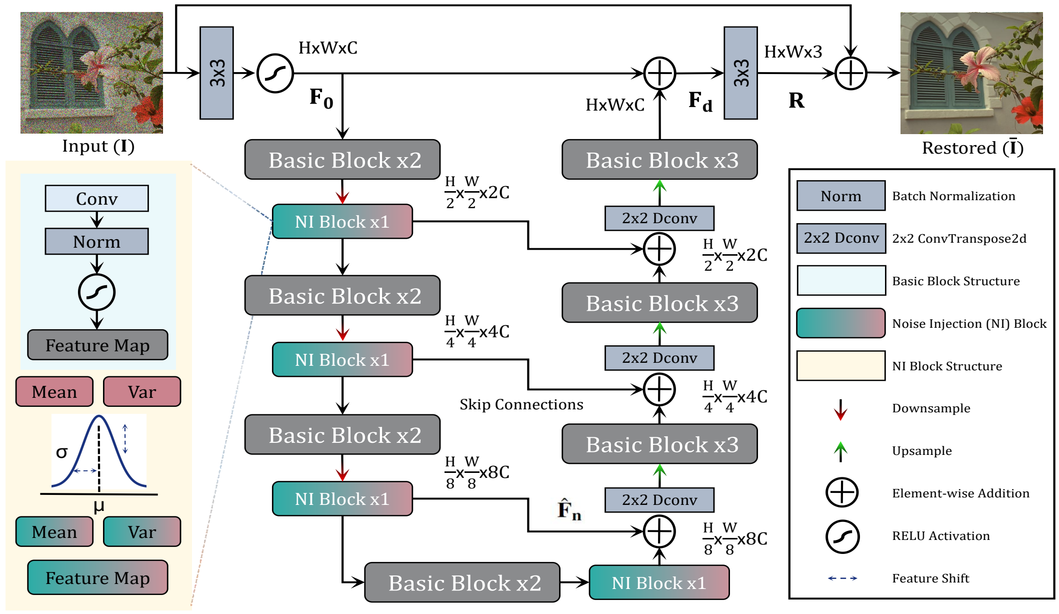

Figure 3: **Overview of RNINet.** Our model consists of a streamlined hierarchical encoder-decoder architecture that integrates basic blocks and noise injection blocks. The basic blocks function as feature extractors within both encoder and decoder stages. Noise injection blocks enhance generalization capabilities by injecting random noise into the feature statistics in the encoder stage.

3 METHOD

3.1 OVERALL PIPELINE

The overall structure of RNINet is depicted in Fig. 3. In the general inference manifold, given a noisy input image $\mathbf{I} \in \mathbb{R}^{H\times W\times 3}$, our proposed RNINet commences by extracting low-level features $\mathbf{F_0} \in \mathbb{R}^{H\times W\times C}$ through a convolution operation followed by a ReLU activation function, where $H\times W$ represents the spatial resolution, and C denotes the number of channels. Subsequently, these feature embeddings $\mathbf{F_0}$ are processed via a four-level hierarchical encoder-decoder structure to transform into deep features $\mathbf{F_d} \in \mathbb{R}^{H\times W\times C}$. Each encoder-decoder level incorporates multiple basic blocks, each consisting of a convolution layer, a batch normalization layer, and a ReLU activation layer. The encoder progressively reduces spatial resolution while enhancing channel capacity, culminating in a low-resolution latent representation $\hat{\mathbf{F}}_\mathbf{n}$. To facilitate the encoding process, noise injection blocks are strategically integrated at every two levels of the encoder. These blocks obtain noised feature statistics $\hat{\mathbf{F}}_\mathbf{n}$ by injecting random noise tensors. The decoder's objective is to incrementally reconstruct the high-resolution clean output from $\hat{\mathbf{F}}_\mathbf{n}$. Downsampling and upsampling within the features are executed using convolution and transposed convolution, respectively. The refined deep features $\mathbf{F_d}$ are subsequently processed through a final convolution layer to produce a residual image $\mathbf{R} \in \mathbb{R}^{H\times W\times 3}$, which is added to the degraded input to yield the restored image: $\bar{\mathbf{I}} = \mathbf{I} + \mathbf{R}$. Following this, we detail the specific modules comprising the basic and noise injection blocks.

3.2 BASIC BLOCK

To mitigate the risk of overfitting and thereby enhance the generalization capabilities of our denoising model, as indicated by existing studies (Liu et al., 2023; Chen et al., 2023; Liu et al., 2021), we have opted for a straightforward structure for the basic block within our RNINet framework. As depicted in Fig. 3, the basic block consists of three layers and functions as feature extractor at both the encoder and decoder stages of the network. Given the input features $\mathbf{F} \in \mathbb{R}^{B\times H\times W\times C}$, the transformation process facilitated by the basic block is defined by the following equation:

$$\mathbf{F_e} = \mathrm{ReLU}(\mathrm{BN}(\mathrm{Conv}(\mathbf{F}))) \tag{1}$$

where Conv denotes the convolution operation, BN represents batch normalization, and ReLU is the rectified linear unit activation function. This streamlined structure ensures efficient and effective feature extraction, with reduced complexity to prevent overfitting issue.

3.3 NOISE INJECTION BLOCK

The noise injection block is designed to generate noised features with altered statistical properties, enhancing the model's generalization to unseen noise types. Given feature $\mathbf{F_e}$, this block first conducts downsampling via convolution (excluding the final block), after which the features undergo batch normalization and ReLU activation, resulting in $\hat{\mathbf{F}}_\mathbf{e} \in \mathbb{R}^{B\times H^\mathbf{s}\times W^\mathbf{s}\times C^\mathbf{s}}$, where $H^\mathbf{s}, W^\mathbf{s}, C^\mathbf{s}$ denote the new height, width, and channel dimension after downsampling. The downsampling step increases the channel dimension, aiding in the computation of feature statistics in the subsequent process. Random noises are then injected into these statistics to generate features with altered characteristics.

3.3.1 FEATURE STATISTICS

Building on prior research (Huang & Belongie, 2017; Li et al., 2021), we recognize that feature statistics, specifically the mean and standard deviation, retain informative properties of a domain. We compute these statistics for the downsampled feature representation $\hat{\mathbf{F}}_\mathbf{e}$, where $\mu \in \mathbb{R}^{B\times C^\mathbf{s}}$ and $\sigma \in \mathbb{R}^{B\times C^\mathbf{s}}$ represent the channel-wise mean and standard deviation of each instance in a batch, respectively:

$$\mu = \frac{1}{H^\mathbf{s} W^\mathbf{s}} \sum_{h=1}^{H^\mathbf{s}} \sum_{w=1}^{W^\mathbf{s}} \hat{\mathbf{F}}_\mathbf{e} \tag{2}$$

$$\sigma^2 = \frac{1}{H^\mathbf{s} W^\mathbf{s}} \sum_{h=1}^{H^\mathbf{s}} \sum_{w=1}^{W^\mathbf{s}} (\hat{\mathbf{F}}_\mathbf{e} - \mu)^2 \tag{3}$$

Before injecting noise, we standardize the features using Z-score normalization. This step is crucial as it prepares the baseline features by aligning the distribution around a zero mean and unit variance, ensuring the consistency of baseline features in subsequent manipulations. The normalized features, denoted as $\hat{\mathbf{F}}_\mathbf{z}$, are calculated as follows:

$$\hat{\mathbf{F}}_\mathbf{z} = (\hat{\mathbf{F}}_\mathbf{e} - \mu)/\sigma \tag{4}$$

3.3.2 REPARAMETERIZATION AS NOISE INJECTION

Reparameterization is a technique to render the sampling operation differentiable. In our approach, we reshape the reparameterization as noise injection operation which involves sampling a latent variable using a deterministic function that incorporates the mean, variance, and an auxiliary variable from a standard distribution. Specifically, we sample two random noise tensors: $\varepsilon_1 \in \mathbb{R}^{B\times C^\mathbf{s}}$ and $\varepsilon_2 \in \mathbb{R}^{B\times C^\mathbf{s}}$ from a normal distribution $N(0, 1)$. We then apply a deterministic function follow the format of reparameterization to inject two random noise tensors respectively into the mean and standard deviation of the downsampled feature representation $\hat{\mathbf{F}}_\mathbf{e}$, this process can be formulated as below:

$$\mu^\mathbf{n} = \mu + \varepsilon_1 * V(\mu), \quad \sigma^\mathbf{n} = \sigma + \varepsilon_2 * V(\sigma) \tag{5}$$

The function V calculates the variance across the batch dimension, and * denotes element-wise multiplication. This reparameterization format allows the network to adaptively learn modifications through its parameters during the noise injection process. Using the altered feature statistics, we restore the normalized feature $\hat{\mathbf{F}}_\mathbf{z}$ to obtain the noised feature $\hat{\mathbf{F}}_\mathbf{n}$:

$$\hat{\mathbf{F}}_\mathbf{n} = \hat{\mathbf{F}}_\mathbf{z} * \sigma^\mathbf{n} + \mu^\mathbf{n} \tag{6}$$

To allocate space for more thorough experiments, we have moved the pseudo-code style pipeline (Algorithm 1), along with the technical explanation and proof part, to Appendix A.3. Please refer to this appendix for comprehensive details. The encoding process in our model integrates varied semantic information from low-level to high-level characteristics during model learning. To enhance performance, noise injection block is applied at each encoding level, for a total of four times. The resultant noised feature $\hat{\mathbf{F}}_{\mathbf{n}}$ possesses significantly altered feature statistics, containing potential domain information from various unseen noise types—crucial for robust model generalization.

4 EXPERIMENTS

Implementation Details. Our RNINet framework comprises a 4-level encoder-decoder setup. Channel counts across these levels are [64, 128, 256, 512]. In the basic blocks, the convolution layers have a kernel size of 3, while in the noise injection blocks, the downsampling convolution layers feature a kernel size of 2 with a stride of 2. Following the state-of-the-art methodology outlined in MT (Chen et al., 2023), we train our model exclusively with Gaussian noise characterized by a standard deviation of $\sigma = 15$. The testing involves noise types not seen during training. Our training dataset amalgamates DIV2K (Agustsson et al., 2017), Flickr2k (Timofte et al., 2017), BSD400 (Arbeláez et al., 2011), and WED (Ma et al., 2017). All experimental procedures are executed using the PyTorch framework on an RTX 4090 GPU. Training employs the Adam optimizer with $\beta_1 = 0.9$ and $\beta_2 = 0.999$. The learning rate is maintained at 1×10^{-4} with a batch size of 8. The training process spans 50,000 iterations, as extending beyond this count might lead to the overfitting of Gaussian noise. For data augmentation, we apply horizontal and vertical flips and extract random 128×128 patches.

Testing Noise. Despite being trained solely on Gaussian noise, the model's generalization capabilities are tested against seven other types of noise: (1) Speckle Noise (2) Salt & Pepper Noise (3) Poisson Noise (4) Image Signal Processing (ISP) Noise (Brooks et al., 2019a). (5) Mixture Noise obtained by mixing the above different types of noise with different levels. The clean images origins from four benchmark datasets: McMaster (Zhang et al., 2011), Kodak24 (Franzen, 1999), CBSD68 (Martin et al., 2001), Urban100 (Huang et al., 2015). We also include two real noise types in our experiments: (6) Monte Carlo Rendering Image Noise and (7) Smartphone Image Noise (Abdelhamed et al., 2018a). Further details on these noise types are provided in the Appendix A.1. For performance evaluation, we employ metrics such as Peak Signal-to-Noise Ratio (PSNR) and Structural Similarity Index Measure (SSIM).

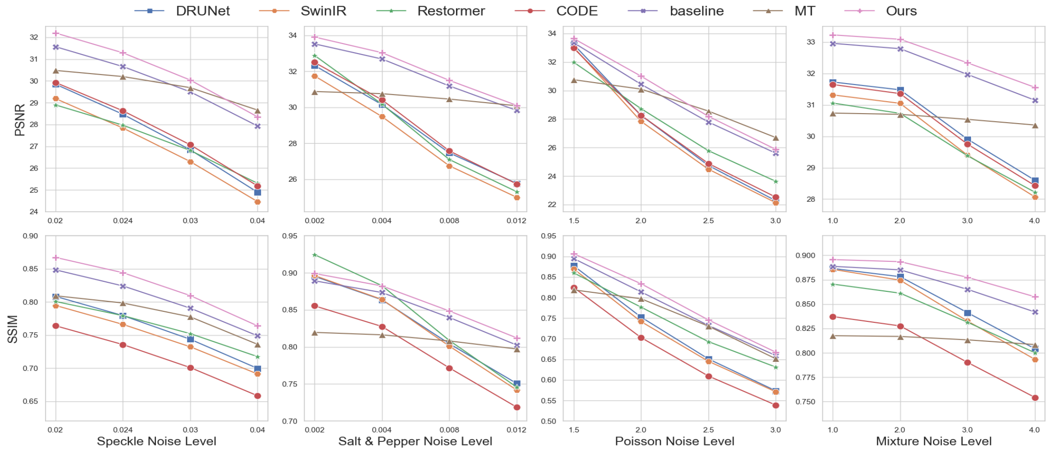

Figure 4: Performance comparisons on four noise types with different levels on the McMaster dataset (Zhang et al., 2011). All models are trained only on Gaussian noise $\sigma = 15$. Our RNINet demonstrates good generalization performance across different noise types. The quantitative results can be found in Tab. 9 in Appendix. For more results on other testsets: Kodak24 (Franzen, 1999), CBSD68 (Martin et al., 2001),Urban100 (Huang et al., 2015), please refer to Appendix A.2.

4.1 THE GENERALIZATION PERFORMANCE

Our model was trained exclusively on Gaussian noise with $\sigma = 15$, yet it was tested on a range of unencountered non-Gaussian noises to assess its generalization capability. We compared our model with other state-of-the-art models that are not generalizable: SwinIR (Liang et al., 2021), Restormer (Zamir et al., 2022), CODE (Zhao et al., 2023), DRUNet (Zhang et al., 2022), and also with the current state-of-the-art method for generalizable deep image denoising: Masked Training (MT) (Chen et al., 2023), under consistent experimental settings. Additionally, we report on a baseline model where noise injection blocks were substituted with basic blocks. As depicted in Fig. 4 and Tab. 9 in the Appendix, our model consistently outperforms others in terms of generalization performance across various tests. Specifically, in scenarios with speckle noise at $\sigma^2 = 0.02$ and $\sigma^2 = 0.024$, our RNINet registered a PSNR improvement of 1.72 dB and 1.09 dB over MT, and 0.63 dB over the baseline model, respectively. The diminished performance of MT (Chen et al., 2023) can be attributed to its design, which tends to result in over-smoothed images. Although MT's masking strategy yields competitive results in highly noisy conditions (*e.g.*, $\sigma^2 = 0.04$), it falls short in scenarios with moderate noise levels. Besides, our method significant outperforms MT in handling mixture noises, which are more complicated and representative in real application environments. Visual comparisons in Fig. 5 further demonstrate that our model yields comparable denoising outcomes compared to both non-generalizable models and the generalizable model.

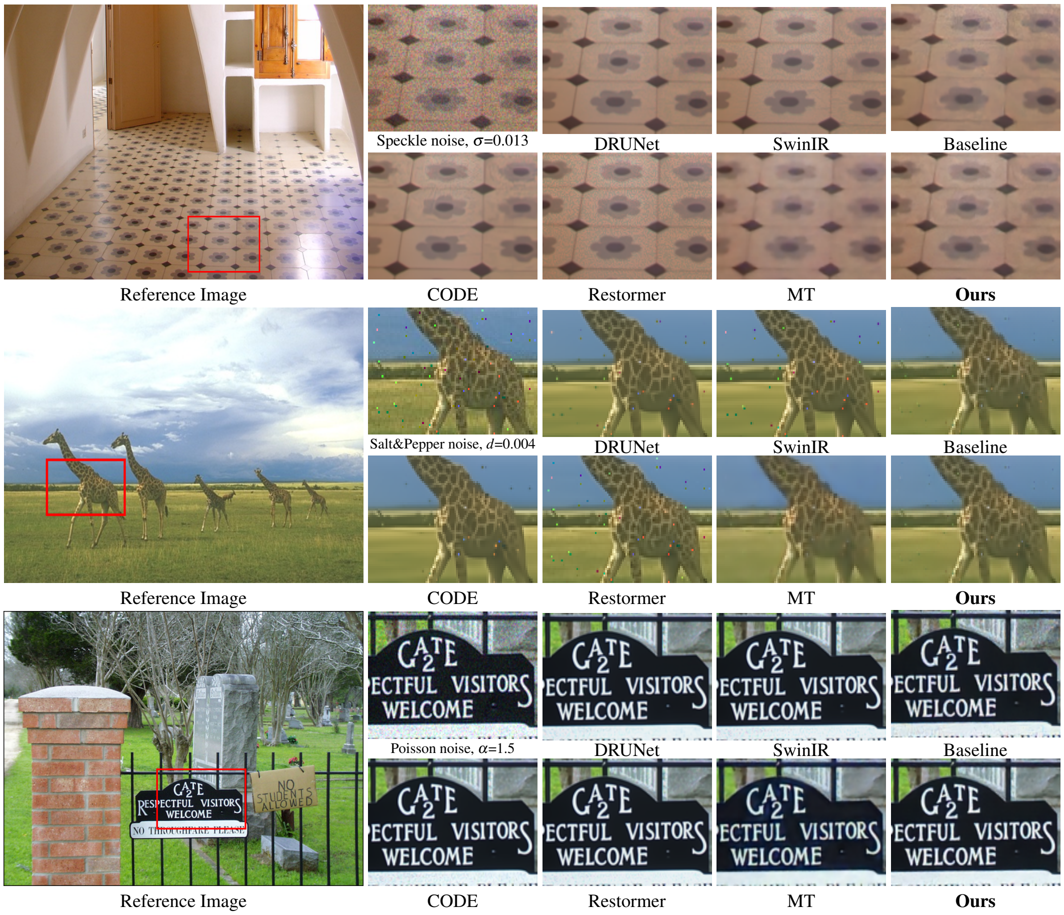

Figure 5: Visual comparisons on out-of-distribution noises. Our RNINet is trained only on Gaussian noise but can generalize well to other unseen noises. Compared with MT (Chen et al., 2023) which generates over-smoothed content, our model can preserve more details, therefore leading to higher PSNR and SSIM.

4.2 EVALUATION ON MONTE CARLO RENDERING NOISE REMOVAL

We extend our evaluation to include the removal of noise from Monte Carlo rendering, consistent with MT (Chen et al., 2023). Monte Carlo denoising is a critical component of the rendering process, especially given the prevalent use of Monte Carlo rendering algorithms in the industry (Burley et al., 2018; Christensen et al., 2018; Kulla et al., 2018). We utilize the test dataset proposed by (Firmino et al., 2022) and convert the raw dataset to the sRGB color space for our Monte Carlo rendered image denoising experiments. The test images were rendered at varying levels of samples per pixel (spp): 256 spp, 128 spp, and 64 spp. Notably, the lower the spp, the higher the noise intensity in the images. Tab. 1 and Fig. 6 display the denoising results. Our method demonstrates superior performance across all settings (256 spp, 128 spp, and 64 spp) and produces visually more appealing images with reduced noise and enhanced details.

	256 Samples Per Pixel		**128 Samples Per Pixel**		**64 Samples Per Pixel**	
Method	PSNR↑	SSIM↑	PSNR↑	SSIM↑	PSNR↑	SSIM↑
DRUNet (Zhang et al., 2022)	33.12	0.8656	29.78	0.7882	26.70	0.7068
SwinIR (Liang et al., 2021)	33.09	0.8566	29.70	0.7767	26.54	0.6948
Restormer (Zamir et al., 2022)	28.48	0.7342	27.08	0.6578	25.76	0.6620
CODE (Zhao et al., 2023)	31.98	0.7815	29.14	0.6995	26.28	0.6138
Baseline	32.69	0.8630	29.74	0.7940	27.12	0.7134
MT (Chen et al., 2023)	30.32	0.7769	28.87	0.7219	26.78	0.6349
Ours	**33.36**	**0.8760**	**30.34**	**0.8056**	**27.38**	**0.7244**

Table 1: Quantitative comparisons on Monte Carlo rendering image denoising.

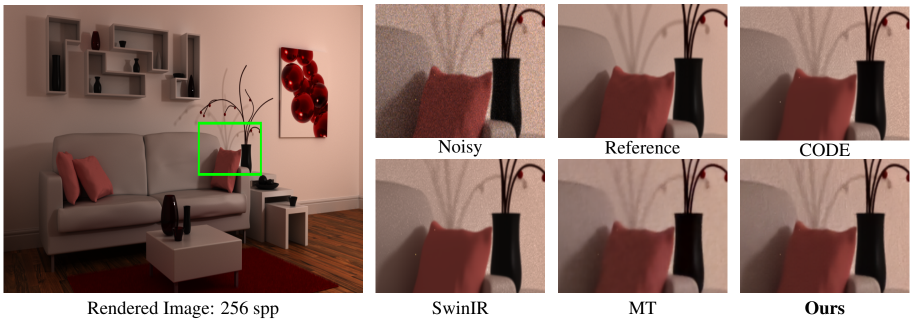

Figure 6: Visual comparisons on Monte Carlo rendering noise removal.

4.3 EVALUATION ON ISP NOISE REMOVAL

Aligned with the current state-of-the-art, MT (Chen et al., 2023), we have conducted evaluations of our model on ISP noise removal to assess its practical significance. Utilizing the systematic approach proposed by Brooks et al. (Brooks et al., 2019a) for generating realistic raw data with ISP noise, we applied the default parameter settings from their research to synthesize ISP noise using the McMaster dataset (Zhang et al., 2011) for our experiments. The comparative results, presented in Tab. 2, demonstrate that our method not only outperforms other models but also surpasses the MT (Chen et al., 2023) benchmark by 1 dB in PSNR, despite a minor reduction in SSIM. The visualizations shown in Fig. 7 further highlight our model's capability to preserve image detail while effectively mitigating ISP noise, confirming its robustness in this domain.

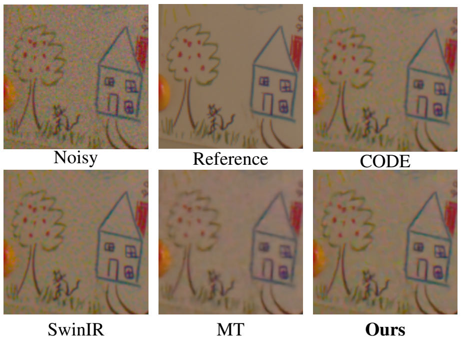

Figure 7: Visual comparisons on synthetic ISP noise removal. Our method can remove noise and preserve more details, therefore leading to higher PSNR and SSIM.

4.4 EVALUATION ON SMARTPHONE IMAGE NOISE REMOVAL

In addition to Monte Carlo rendering noise, our study addresses another real-world noise type: Smartphone Image Noise. The Smartphone Image Denoising Dataset (SIDD) (Abdelhamed et al., 2018a) includes images from 10 different scenes captured under various lighting conditions using five representative cameras. Testing the generalization performance of models on the SIDD validation dataset is particularly challenging due to the complexity of the noise and the requirement that models must not have prior information about the noise distributions in SIDD for a fair generalization test.

Method	Synthetic ISP Noise PSNR↑	Synthetic ISP Noise SSIM↑
DRUNet (Zhang et al., 2022)	31.01	0.8033
SwinIR (Liang et al., 2021)	31.09	0.7968
Restormer (Zamir et al., 2022)	26.02	0.6762
CODE (Zhao et al., 2023)	30.59	0.7908
Baseline	30.99	0.8129
MT (Chen et al., 2023)	30.15	0.8232
Ours	**31.15**	**0.8195**

Table 2: Quantitative comparisons on synthetic ISP noise removal.

Method	Smartphone Image Noise PSNR↑	Smartphone Image Noise SSIM↑
DRUNet (Zhang et al., 2022)	28.09	0.5726
SwinIR (Liang et al., 2021)	27.62	0.5604
Restormer (Zamir et al., 2022)	22.54	0.3700
CODE (Zhao et al., 2023)	26.81	0.5186
Baseline	28.64	0.5953
MT (Chen et al., 2023)	28.66	0.6044
Ours	**28.90**	**0.6041**

Table 3: Quantitative comparisons on smartphone image noise removal.

As shown in Tab. 3, our method achieves significant improvements in PSNR (+0.24 dB than MT (Chen et al., 2023)) over competing methods even under these stringent conditions. The visual results, presented in Fig. 8, demonstrate that while the MT method tends to oversmooth content, resulting in unclear edges, neither CODE nor SwinIR effectively reduce the appearance of black cyan noise spots, but our model can preserve image detail while effectively reducing noise. It is crucial to note that we had no access to the images from the training or testing portions of the SIDD prior to testing, meaning we lacked prior information about the image content and noise distribution within the dataset. Although some supervised methods (Chen et al., 2022a; Yue et al., 2020; Jang et al., 2024) have demonstrated superior results on SIDD, their models can not generalize as effectively to other noise types as our RNINet does due to that they are still overfitting the noise in SIDD dataset.

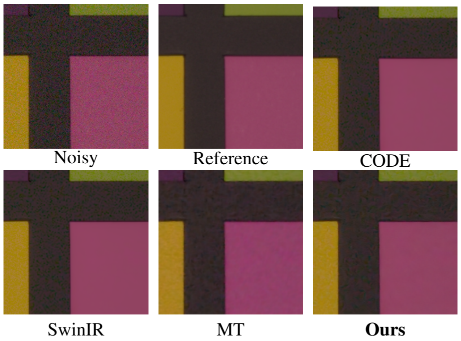

Figure 8: Visual comparisons on smartphone image noise removal. Our method can remove noise and preserve more details, therefore leading to higher PSNR and SSIM.

4.5 In Distribution Performance Comparison

Our method has shown promising results on unseen noise types, highlighting its excellent generalization capabilities, it is equally important to assess performance on in-distribution noise. Therefore, we conducted a comparative analysis with the state-of-the-art generalizable method MT (Chen et al., 2023), which is also trained on single Gaussian noise with $\sigma = 15$. Following the Gaussian denoise benchmark criteria outlined in (Liang et al., 2021; Zamir et al., 2022; Zhao et al., 2023), we tested both MT and our RNINet on four testsets: McMaster (Zhang et al., 2011), Kodak24 (Franzen, 1999), CBSD68 (Martin et al., 2001), Urban100 (Huang et al., 2015). As illustrated in Tab. 4, our method significantly outperforms MT in both PSNR and SSIM, with improvements in PSNR ranging from a minimum of 2.46 dB to a maximum of 3.46 dB. MT's underperformance in in-distribution conditions can be attributed to its masking operation, which tends to overly smooth image content to achieve better generalization. In contrast, our method not only delivers good generalization performance but also excels in in-distribution denoising scenarios, further demonstrating the robustness of our noise removal approach.

4.6 MACs, GPU Memory Usage and Runtime

Resource efficiency is crucial when deploying generalizable denoising models in real-world applications. Therefore, we report on MACs, GPU memory cost, and runtime comparisons between MT (Chen et al., 2023) and our RNINet. As indicated in Tab. 5, RNINet demonstrates significantly lower MACs, reduced GPU memory usage, and faster runtime, attributable to our model's simplified architectural design. Unlike MT, which employs a complex masked swinir structure leading to higher resource consumption and longer runtimes, RNINet offers superior resource cost efficiency alongside enhanced general denoising performance. This makes RNINet particularly suitable for applications requiring efficient operation without compromising on denoising quality.

	MT		Ours	
Dataset	PSNR↑	SSIM↑	PSNR↑	SSIM↑
McMaster	30.85	0.8325	**34.05**$_{\uparrow 3.20}$	**0.9122**$_{\uparrow 0.0797}$
Kodak24	31.65	0.8836	**34.11**$_{\uparrow 2.46}$	**0.9128**$_{\uparrow 0.0292}$
CBSD68	31.00	0.8880	**33.50**$_{\uparrow 2.50}$	**0.9217**$_{\uparrow 0.0337}$
Urban100	29.51	0.8992	**32.97**$_{\uparrow 3.46}$	**0.9310**$_{\uparrow 0.0318}$

Table 4: Quantitative comparisons on in-distribution denoising performance. Our method significantly outperforms MT (Chen et al., 2023) in both PSNR and SSIM across four benchmark datasets. The ↑ indicates the absolute improvement over MT, highlighting the robust in-distribution denoising capability of our approach.

Metrics	MT	**Ours**
MACs	51.6G	**44.7G**$_{\downarrow 0.87\times}$
GPU Memory Usage	0.90G	**0.62G**$_{\downarrow 0.69\times}$
Runtime	1.04s	**0.10s**$_{\downarrow 0.10\times}$

Table 5: Quantitative comparisons on MACs, GPU memory usage and runtime. MACs and GPU memory usage were tested on images of size 256 × 256. Runtime was tested by calculating the average inference time per image in McMaster testset. The ↓ denotes the relative rate compared with MT, highlighting the efficiency of our method.

4.7 GENERALIZATION ANALYSIS

Following (Kong et al., 2022; Wang et al., 2024), we utilize the Deep Degradation Representation (DDR) introduced by (Liu et al., 2021) and visualize it in Fig. 9. DDR enables us to probe the network's generalization capabilities by analyzing model behavior across different degradations. In our cases, each point corresponds to an input image, with different colors denoting various noise types. For instance, in the cases of SwinIR and Restormer, it is noticeable that images with identical noise types tend to cluster together, suggesting that these models may encode noise-specific information, potentially leading to an overfitting issue. Nevertheless, the points in MT and our method are clustered based on their content rather than noise type. (Liu et al., 2021) also employs the Calinski-Harabaz Index (CHI) score for a more quantitative analysis of clustering efficiency, where a lower CHI score indicates better cluster separation and, consequently, superior generalization ability. Notably, both MT and our method achieve very low CHI scores; however, our method's CHI score is still significantly lower than that of MT, which underscores our model's enhanced generalization performance.

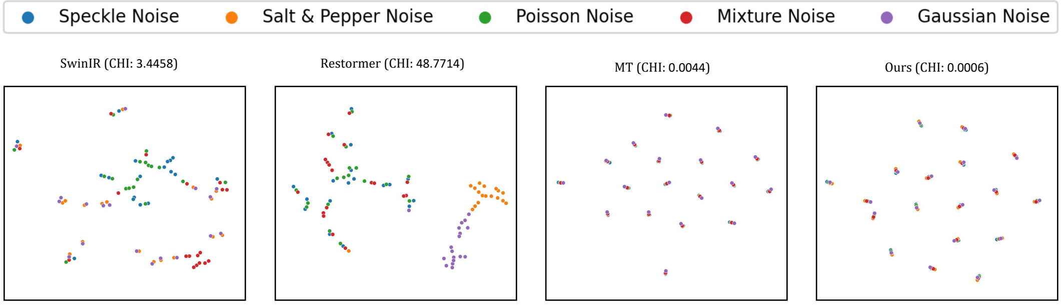

Figure 9: Visualization of the DDR clusters for generalization analysis. A lower CHI score demonstrates better cluster separation, which in turn suggests superior generalization capability.

5 CONCLUSION

In this work, we introduce RNINet, a novel architecture designed for generalizable deep image denoising. RNINet incorporates a streamlined encoder-decoder framework with noise injection blocks, addressing the prevalent issue of over-smoothing observed in the existing MT method, while also enhancing both efficiency and overall performance. Our approach leverages the insight that feature statistics, such as the mean and variance of a denoising model, shift significantly in response to different noise types used during training. To exploit this, we introduce a noise injection block within our framework that injects random noise into the feature statistics, significantly improving generalization across unseen noise types. Extensive experimental results demonstrate that RNINet not only surpasses the state-of-the-art MT method in terms of denoising effectiveness and computational efficiency but also achieves inference speeds up to ten times faster. This study not only advances the field of generalizable deep image denoising but also paves the way for future research into broader applications of robust noise-handling models.

REFERENCES

Abdelrahman Abdelhamed, Stephen Lin, and Michael S Brown. A high-quality denoising dataset for smartphone cameras. In *Proceedings of the IEEE conference on computer vision and pattern recognition*, pp. 1692–1700, 2018a.

Abdelrahman Abdelhamed, Stephen Lin, and Michael S Brown. A high-quality denoising dataset for smartphone cameras. In *Proceedings of the IEEE conference on computer vision and pattern recognition*, pp. 1692–1700, 2018b.

Agustsson et al. Ntire 2017 challenge on single image super-resolution: Dataset and study. In *Proceedings of the IEEE Conference on Computer Vision and Pattern Recognition (CVPR) Workshops*, July 2017.

Pablo Arbeláez, Michael Maire, Charless Fowlkes, and Jitendra Malik. Contour detection and hierarchical image segmentation. *IEEE Transactions on Pattern Analysis and Machine Intelligence*, 33(5):898–916, 2011. doi: 10.1109/TPAMI.2010.161.

Tim Brooks, Ben Mildenhall, Tianfan Xue, Jiawen Chen, Dillon Sharlet, and Jonathan T Barron. Unprocessing images for learned raw denoising. In *Proceedings of the IEEE/CVF conference on computer vision and pattern recognition*, pp. 11036–11045, 2019a.

Tim Brooks, Ben Mildenhall, Tianfan Xue, Jiawen Chen, Dillon Sharlet, and Jonathan T Barron. Unprocessing images for learned raw denoising. In *Proceedings of the IEEE/CVF conference on computer vision and pattern recognition*, pp. 11036–11045, 2019b.

Antoni Buades, Bartomeu Coll, and J-M Morel. A non-local algorithm for image denoising. In *2005 IEEE computer society conference on computer vision and pattern recognition (CVPR'05)*, volume 2, pp. 60–65. Ieee, 2005.

Brent Burley, David Adler, Matt Jen-Yuan Chiang, Hank Driskill, Ralf Habel, Patrick Kelly, Peter Kutz, Yining Karl Li, and Daniel Teece. The design and evolution of disney's hyperion renderer. *ACM Transactions on Graphics (TOG)*, 37(3):1–22, 2018.

Hanting Chen, Yunhe Wang, Tianyu Guo, Chang Xu, Yiping Deng, Zhenhua Liu, Siwei Ma, Chunjing Xu, Chao Xu, and Wen Gao. Pre-trained image processing transformer. In *Proceedings of the IEEE/CVF conference on computer vision and pattern recognition*, pp. 12299–12310, 2021.

Haoyu Chen, Jinjin Gu, Yihao Liu, Salma Abdel Magid, Chao Dong, Qiong Wang, Hanspeter Pfister, and Lei Zhu. Masked image training for generalizable deep image denoising. In *Proceedings of the IEEE/CVF Conference on Computer Vision and Pattern Recognition*, pp. 1692–1703, 2023.

Jingwen Chen, Jiawei Chen, Hongyang Chao, and Ming Yang. Image blind denoising with generative adversarial network based noise modeling. In *Proceedings of the IEEE conference on computer vision and pattern recognition*, pp. 3155–3164, 2018.

Liangyu Chen, Xiaojie Chu, Xiangyu Zhang, and Jian Sun. Simple baselines for image restoration. *arXiv preprint arXiv:2204.04676*, 2022a.

Zheng Chen, Yulun Zhang, Jinjin Gu, Linghe Kong, Xin Yuan, et al. Cross aggregation transformer for image restoration. *Advances in Neural Information Processing Systems*, 35:25478–25490, 2022b.

Jun Cheng, Dong Liang, and Shan Tan. Transfer clip for generalizable image denoising. In *Proceedings of the IEEE/CVF Conference on Computer Vision and Pattern Recognition*, pp. 25974–25984, 2024.

Per Christensen, Julian Fong, Jonathan Shade, Wayne Wooten, Brenden Schubert, Andrew Kensler, Stephen Friedman, Charlie Kilpatrick, Cliff Ramshaw, Marc Bannister, et al. Renderman: An advanced path-tracing architecture for movie rendering. *ACM Transactions on Graphics (TOG)*, 37(3):1–21, 2018.

Kostadin Dabov, Alessandro Foi, Vladimir Katkovnik, and Karen Egiazarian. Image denoising by sparse 3-d transform-domain collaborative filtering. *IEEE Transactions on image processing*, 16 (8):2080–2095, 2007.

Nithish Divakar and R Venkatesh Babu. Image denoising via cnns: An adversarial approach. In *Proceedings of the IEEE Conference on Computer Vision and Pattern Recognition Workshops*, pp. 80–87, 2017.

Alexey Dosovitskiy, Lucas Beyer, Alexander Kolesnikov, Dirk Weissenborn, Xiaohua Zhai, Thomas Unterthiner, Mostafa Dehghani, Matthias Minderer, Georg Heigold, Sylvain Gelly, et al. An image is worth 16x16 words: Transformers for image recognition at scale. *arXiv preprint arXiv:2010.11929*, 2020.

Michael Elad and Michal Aharon. Image denoising via sparse and redundant representations over learned dictionaries. *IEEE Transactions on Image processing*, 15(12):3736–3745, 2006.

Arthur Firmino, Jeppe Revall Frisvad, and Henrik Wann Jensen. Progressive denoising of monte carlo rendered images. In *Computer Graphics Forum*, volume 41, pp. 1–11. Wiley Online Library, 2022.

Rich Franzen. Kodak lossless true color image suite. *source: http://r0k. us/graphics/kodak*, 4(2):9, 1999.

Shang-Hua Gao, Qi Han, Duo Li, Ming-Ming Cheng, and Pai Peng. Representative batch normalization with feature calibration. In *Proceedings of the IEEE/CVF conference on computer vision and pattern recognition*, pp. 8669–8679, 2021.

Shuhang Gu, Lei Zhang, Wangmeng Zuo, and Xiangchu Feng. Weighted nuclear norm minimization with application to image denoising. In *Proceedings of the IEEE conference on computer vision and pattern recognition*, pp. 2862–2869, 2014.

Shi Guo, Zifei Yan, Kai Zhang, Wangmeng Zuo, and Lei Zhang. Toward convolutional blind denoising of real photographs. In *Proceedings of the IEEE/CVF conference on computer vision and pattern recognition*, pp. 1712–1722, 2019.

Jin Han, Yixin Yang, Peiqi Duan, Chu Zhou, Lei Ma, Chao Xu, Tiejun Huang, Imari Sato, and Boxin Shi. Hybrid high dynamic range imaging fusing neuromorphic and conventional images. *IEEE Transactions on Pattern Analysis and Machine Intelligence*, 45(7):8553–8565, 2023. doi: 10.1109/TPAMI.2022.3231334.

Xun Huang and Serge Belongie. Arbitrary style transfer in real-time with adaptive instance normalization. In *Proceedings of the IEEE international conference on computer vision*, pp. 1501–1510, 2017.

Huang et al. Single image super-resolution from transformed self-exemplars. In *Proceedings of the IEEE Conference on Computer Vision and Pattern Recognition (CVPR)*, June 2015.

Sergey Ioffe and Christian Szegedy. Batch normalization: Accelerating deep network training by reducing internal covariate shift. In *International conference on machine learning*, pp. 448–456. pmlr, 2015.

Hyemi Jang, Junsung Park, Dahuin Jung, Jaihyun Lew, Ho Bae, and Sungroh Yoon. Puca: patch-unshuffle and channel attention for enhanced self-supervised image denoising. *Advances in Neural Information Processing Systems*, 36, 2024.

Xixi Jia, Sanyang Liu, Xiangchu Feng, and Lei Zhang. Focnet: A fractional optimal control network for image denoising. In *Proceedings of the IEEE/CVF conference on computer vision and pattern recognition*, pp. 6054–6063, 2019.

Changjin Kim, Tae Hyun Kim, and Sungyong Baik. Lan: Learning to adapt noise for image denoising. In *Proceedings of the IEEE/CVF Conference on Computer Vision and Pattern Recognition*, pp. 25193–25202, 2024.

Xiangtao Kong, Xina Liu, Jinjin Gu, Yu Qiao, and Chao Dong. Reflash dropout in image super-resolution. In *Proceedings of the IEEE/CVF Conference on Computer Vision and Pattern Recognition*, pp. 6002–6012, 2022.

Alexander Krull, Tim-Oliver Buchholz, and Florian Jug. Noise2void - learning denoising from single noisy images. In *IEEE Conference on Computer Vision and Pattern Recognition, CVPR 2019, Long Beach, CA, USA, June 16-20, 2019*, pp. 2129–2137. Computer Vision Foundation / IEEE, 2019. doi: 10.1109/CVPR.2019.00223. URL `http://openaccess.thecvf.com/content_CVPR_2019/html/Krull_Noise2Void_-_Learning_Denoising_From_Single_Noisy_Images_CVPR_2019_paper.html`.

Christopher Kulla, Alejandro Conty, Clifford Stein, and Larry Gritz. Sony pictures imageworks arnold. *ACM Transactions on Graphics (TOG)*, 37(3):1–18, 2018.

Stamatios Lefkimmiatis. Non-local color image denoising with convolutional neural networks. In *Proceedings of the IEEE conference on computer vision and pattern recognition*, pp. 3587–3596, 2017.

Stamatios Lefkimmiatis. Universal denoising networks: a novel cnn architecture for image denoising. In *Proceedings of the IEEE conference on computer vision and pattern recognition*, pp. 3204–3213, 2018.

Boyi Li, Felix Wu, Ser-Nam Lim, Serge Belongie, and Kilian Q Weinberger. On feature normalization and data augmentation. In *Proceedings of the IEEE/CVF conference on computer vision and pattern recognition*, pp. 12383–12392, 2021.

Xiaotong Li, Yongxing Dai, Yixiao Ge, Jun Liu, Ying Shan, and Ling-Yu Duan. Uncertainty modeling for out-of-distribution generalization. *arXiv preprint arXiv:2202.03958*, 2022.

Jingyun Liang, Jiezhang Cao, Guolei Sun, Kai Zhang, Luc Van Gool, and Radu Timofte. Swinir: Image restoration using swin transformer. In *Proceedings of the IEEE/CVF international conference on computer vision*, pp. 1833–1844, 2021.

Yihao Liu, Anran Liu, Jinjin Gu, Zhipeng Zhang, Wenhao Wu, Yu Qiao, and Chao Dong. Discovering distinctive" semantics" in super-resolution networks. *arXiv preprint arXiv:2108.00406*, 2021.

Yihao Liu, Hengyuan Zhao, Jinjin Gu, Yu Qiao, and Chao Dong. Evaluating the generalization ability of super-resolution networks. *IEEE Transactions on pattern analysis and machine intelligence*, 2023.

Kede Ma, Zhengfang Duanmu, Qingbo Wu, Zhou Wang, Hongwei Yong, Hongliang Li, and Lei Zhang. Waterloo exploration database: New challenges for image quality assessment models. *IEEE Transactions on Image Processing*, 26(2):1004–1016, 2017. doi: 10.1109/TIP.2016.2631888.

Julien Mairal, Francis Bach, Jean Ponce, Guillermo Sapiro, and Andrew Zisserman. Non-local sparse models for image restoration. In *2009 IEEE 12th international conference on computer vision*, pp. 2272–2279. IEEE, 2009.

Xiaojiao Mao, Chunhua Shen, and Yu-Bin Yang. Image restoration using very deep convolutional encoder-decoder networks with symmetric skip connections. *Advances in neural information processing systems*, 29, 2016.

D. Martin, C. Fowlkes, D. Tal, and J. Malik. A database of human segmented natural images and its application to evaluating segmentation algorithms and measuring ecological statistics. In *Proceedings Eighth IEEE International Conference on Computer Vision. ICCV 2001*, volume 2, pp. 416–423 vol.2, 2001. doi: 10.1109/ICCV.2001.937655.

Seonghyeon Nam, Youngbae Hwang, Yasuyuki Matsushita, and Seon Joo Kim. A holistic approach to cross-channel image noise modeling and its application to image denoising. In *Proceedings of the IEEE conference on computer vision and pattern recognition*, pp. 1683–1691, 2016.

Tobias Plotz and Stefan Roth. Benchmarking denoising algorithms with real photographs. In *Proceedings of the IEEE conference on computer vision and pattern recognition*, pp. 1586–1595, 2017.

Radu Timofte, Eirikur Agustsson, Luc Van Gool, Ming-Hsuan Yang, and Lei Zhang. Ntire 2017 challenge on single image super-resolution: Methods and results. In *Proceedings of the IEEE Conference on Computer Vision and Pattern Recognition (CVPR) Workshops*, July 2017.

Hongjun Wang, Jiyuan Chen, Yinqiang Zheng, and Tieyong Zeng. Navigating beyond dropout: An intriguing solution towards generalizable image super resolution. In *Proceedings of the IEEE/CVF Conference on Computer Vision and Pattern Recognition*, pp. 25532–25543, 2024.

Ximei Wang, Ying Jin, Mingsheng Long, Jianmin Wang, and Michael I Jordan. Transferable normalization: Towards improving transferability of deep neural networks. *Advances in neural information processing systems*, 32, 2019.

Zhendong Wang, Xiaodong Cun, Jianmin Bao, Wengang Zhou, Jianzhuang Liu, and Houqiang Li. Uformer: A general u-shaped transformer for image restoration. In *Proceedings of the IEEE/CVF conference on computer vision and pattern recognition*, pp. 17683–17693, 2022.

Kaixuan Wei, Ying Fu, Jiaolong Yang, and Hua Huang. A physics-based noise formation model for extreme low-light raw denoising. In *Proceedings of the IEEE/CVF Conference on Computer Vision and Pattern Recognition*, pp. 2758–2767, 2020.

Jun Xu, Hui Li, Zhetong Liang, David Zhang, and Lei Zhang. Real-world noisy image denoising: A new benchmark. *arXiv preprint arXiv:1804.02603*, 2018.

Yuan Yuan, Siyuan Liu, Jiawei Zhang, Yongbing Zhang, Chao Dong, and Liang Lin. Unsupervised image super-resolution using cycle-in-cycle generative adversarial networks. In *Proceedings of the IEEE conference on computer vision and pattern recognition workshops*, pp. 701–710, 2018.

Zongsheng Yue, Hongwei Yong, Qian Zhao, Deyu Meng, and Lei Zhang. Variational denoising network: Toward blind noise modeling and removal. In Hanna M. Wallach, Hugo Larochelle, Alina Beygelzimer, Florence d'Alché-Buc, Emily B. Fox, and Roman Garnett (eds.), *Advances in Neural Information Processing Systems 32: Annual Conference on Neural Information Processing Systems 2019, NeurIPS 2019, December 8-14, 2019, Vancouver, BC, Canada*, pp. 1688–1699, 2019. URL `https://proceedings.neurips.cc/paper/2019/hash/6395ebd0f4b478145ecfbaf939454fa4-Abstract.html`.

Zongsheng Yue, Qian Zhao, Lei Zhang, and Deyu Meng. Dual adversarial network: Toward real-world noise removal and noise generation. In *Computer Vision–ECCV 2020: 16th European Conference, Glasgow, UK, August 23–28, 2020, Proceedings, Part X 16*, pp. 41–58. Springer, 2020.

Syed Waqas Zamir, Aditya Arora, Salman Khan, Munawar Hayat, Fahad Shahbaz Khan, and Ming-Hsuan Yang. Restormer: Efficient transformer for high-resolution image restoration. In *Proceedings of the IEEE/CVF conference on computer vision and pattern recognition*, pp. 5728–5739, 2022.

Jiale Zhang, Yulun Zhang, Jinjin Gu, Jiahua Dong, Linghe Kong, and Xiaokang Yang. Xformer: Hybrid x-shaped transformer for image denoising. *arXiv preprint arXiv:2303.06440*, 2023a.

Kai Zhang, Wangmeng Zuo, Yunjin Chen, Deyu Meng, and Lei Zhang. Beyond a gaussian denoiser: Residual learning of deep cnn for image denoising. *IEEE transactions on image processing*, 26(7): 3142–3155, 2017.

Kai Zhang, Wangmeng Zuo, and Lei Zhang. Ffdnet: Toward a fast and flexible solution for cnn-based image denoising. *IEEE Transactions on Image Processing*, 27(9):4608–4622, 2018.

Kai Zhang, Yawei Li, Wangmeng Zuo, Lei Zhang, Luc Van Gool, and Radu Timofte. Plug-and-play image restoration with deep denoiser prior. *IEEE Transactions on Pattern Analysis and Machine Intelligence*, 44(10):6360–6376, 2022. doi: 10.1109/TPAMI.2021.3088914.

Kai Zhang, Yawei Li, Jingyun Liang, Jiezhang Cao, Yulun Zhang, Hao Tang, Deng-Ping Fan, Radu Timofte, and Luc Van Gool. Practical blind image denoising via swin-conv-unet and data synthesis. *Mach. Intell. Res.*, 20(6):822–836, 2023b. doi: 10.1007/S11633-023-1466-0. URL `https://doi.org/10.1007/s11633-023-1466-0`.

Lei Zhang, Xiaolin Wu, Antoni Buades, and Xin Li. Color demosaicking by local directional interpolation and nonlocal adaptive thresholding. *J. Electronic Imaging*, 20:023016, 2011.

Haiyu Zhao, Yuanbiao Gou, Boyun Li, Dezhong Peng, Jiancheng Lv, and Xi Peng. Comprehensive and delicate: An efficient transformer for image restoration. In *Proceedings of the IEEE/CVF Conference on Computer Vision and Pattern Recognition*, pp. 14122–14132, 2023.

A APPENDIX

A.1 DETAILS OF TEST NOISE

In this section, we provide details on the test noises used in our evaluations:

Speckle Noise: Speckle noise is a granular noise that inherently degrades the quality of images produced by coherent imaging systems such as laser, synthetic aperture radar, and ultrasound. It arises from the random interference of coherent waves scattered by the surface roughness of the target. Following the method outlined in MT (Chen et al., 2023), we use the *imnoise* function in MATLAB to generate speckle noise. The noise level is controlled by the parameter σ^2.

Salt & Pepper Noise: Salt-and-pepper noise is a type of impulse noise characterized by randomly occurring white and black pixels in an image, typically caused by errors in data transmission or malfunctioning camera sensors. As described in MT (Chen et al., 2023), we use the *imnoise* function in MATLAB to generate salt & pepper noise, with the parameter d controlling the noise level.

Poisson Noise: Also known as shot noise, Poisson noise occurs in systems where the signal consists of statistically independent discrete events. This type of noise follows a Poisson distribution and is commonly observed in photon counting processes in optical systems. Following MT (Chen et al., 2023), we amplified the noise using different scaling factors α according to the equation $J = I + n \cdot \alpha$, where n represents the generated Poisson noise, and α is the scaling factor.

Image Signal Processing (ISP) Noise: ISP noise encompasses various types of noise introduced during the process of capturing and converting signals from an image sensor into digital images. This includes noise from sensor readout, fixed pattern noise, dark current noise, and other electronic or thermal interferences. We use the code provided by Brooks et al. (Brooks et al., 2019a) and apply the default settings to convert RGB images to raw format, add ISP noise, and then convert them back to RGB format.

Monte Carlo Rendered Image Noise: Monte Carlo rendered image noise arises in images generated by Monte Carlo rendering techniques, due to the stochastic nature of sampling. Insufficient samples can lead to visible graininess or speckles. We utilize the test dataset proposed by Firmino et al. (Firmino et al., 2022) and convert the raw dataset to the sRGB color space using the code from another study (Han et al., 2023). Unlike MT (Chen et al., 2023), we did not use the tonemapping function when converting raw images to RGB images due to the unavailability of configuration parameters and codes for tonemapping in their work.

Smartphone Image Noise: We utilized the Smartphone Image Denoising Dataset (SIDD) (Abdelhamed et al., 2018a), which comprises images from 10 different scenes captured under various lighting conditions using five representative cameras, to evaluate the generalization capabilities of our RNINet and other methods. We processed the SIDD evaluation data using data preparation codes from NAFNet (Chen et al., 2022a) and directly tested several benchmark methods trained exclusively on Gaussian noise with $\sigma = 15$. It is important to note that we did not have access to any images from the training and testing datasets before testing, which means we had no prior information about the image content and noise distribution within that dataset. While some supervised methods have obtained comparable results on the SIDD evaluation, they can not generalize as well to other noise types as our RNINet does.

Mixture Noise: We simulate real-world noise scenarios by mixing different types of noise with varying intensities, resulting in four levels of mixture noise. The order of noise addition is speckle noise (variance σ_{s1}^2), salt & pepper noise (density d), and Poisson noise (scale α). Unlike MT (Chen et al., 2023), we did not add Gaussian noise, as it is a in-distribution noise that reduces denoising difficulty. The four levels are as follows:

- Level 1: $\sigma_{s1}^2 = 0.003$, $d = 0.002$, $\alpha = 1$
- Level 2: $\sigma_{s1}^2 = 0.004$, $d = 0.002$, $\alpha = 1$
- Level 3: $\sigma_{s1}^2 = 0.006$, $d = 0.003$, $\alpha = 1$
- Level 4: $\sigma_{s1}^2 = 0.008$, $d = 0.004$, $\alpha = 1$

By providing these detailed descriptions and parameters, we aim to ensure the reproducibility and clarity of our noise generation processes.

A.2 ADDITIONAL RESULTS AND ABLATION EXPERIMENTS

Additional ablation experiments. As detailed in Section. 4 and illustrated in our experiment tables, the most important ablation study reported involves a baseline model where noise injection blocks were replaced with basic blocks. Regarding more ablation studies, we adjusted the intensity of random noise injected into feature statistics by applying a scaling factor. The results are presented in Tab. 6. We found that the original scale (no scaling) delivers the best performance compared to other methods. We believe this superior performance is due to the scaling operation disrupting the standard values in the tensors sampled from a Gaussian distribution, thereby degrading the overall performance.

Speckle Noise Scale	$\sigma^2 = 0.02$ PSNR↑/SSIM↑	$\sigma^2 = 0.024$ PSNR↑/SSIM↑	$\sigma^2 = 0.03$ PSNR↑/SSIM↑	$\sigma^2 = 0.04$ PSNR↑/SSIM↑
1.2	31.06/0.8310	29.96/0.8032	28.62/0.7685	26.99/0.7250
1.1	31.20/0.8411	30.20/0.8136	28.87/0.7784	27.18/0.7342
0.9	31.30/0.8335	30.25/0.8076	28.88/0.7738	27.15/0.7295
0.8	31.44/0.8469	30.24/0.8189	28.84/0.7829	27.02/0.7369
1.0 (Original)	**32.20/0.8674**	**31.29/0.8443**	**30.04/0.8097**	**28.35/0.7639**

Table 6: We adjusted the intensity of random noise injected into feature statistics by applying a scaling factor. The experiments demonstrate no scaling delivers the best performance compared to other methods. We believe this superior performance is due to the scaling operation disrupting the standard values in the tensors sampled from a Gaussian distribution, thereby degrading the overall performance.

Additional results on four benchmark datasets. In this section, we first present quantitative results on four benchmark datasets: McMaster (Zhang et al., 2011), CBSD68 (Martin et al., 2001), Kodak24 (Franzen, 1999), and Urban100 (Huang et al., 2015). As shown in Tab. 9, Tab. 10, Tab. 11, and Tab. 12, our RNINet outperforms other state-of-the-art methods in most cases. Specifically, RNINet achieves significantly better performance than other methods for mixture noises in all settings, which are more complicated and representative in real application environments. Besides these significant improvements, our RNINet also demonstrates computational efficiency, with lower MACs and GPU memory usage, RNINet achieves up to 10 times faster inference speeds compared to MT (Chen et al., 2023) as indicated in Tab. 5, making it particularly suitable for applications requiring efficient operation without compromising on denoising quality.

A.3 THEORETICAL EXPLANATION AND PROOF

In this section, we provide a theoretical explanation and proof of our random noise injection strategy, demonstrating why it can improve generalization capability on unseen noise types. This process consists of two steps. In the forward step, we prove that features generated from images with different noise distributions can form a normal distribution. In the backward step, we explain how altered features noised by random tensors sampled from a normal distribution can be mapped through a nonlinear neural network to match features from images with unseen noise types.

Forward: Suppose the neural network N is a complex nonlinear function, with $f_i = N(x_i)$ representing the feature map of an intermediate layer after input x_i passes through the neural network. Assume that for different inputs x_i, their noise distributions follow different distributions such as speckle noise distribution, salt & pepper noise distribution, poisson noise distribution, etc.

According to the Lindeberg-Feller Central Limit Theorem, even if these x_i have different noise distributions, the sum or average of f_i will converge to a normal distribution if certain requirements are met. Due to that x_i are independent but differently distributed, therefore f_i are also independent but differently distributed, a large number of f_i can form a normal distribution. The examination of the four conditions for the Lindeberg-Feller Central Limit Theorem is as follows:

Algorithm 1 Pipeline and Pseudo-code

```
Input: Normal feature $\hat{\mathbf{F}}_\mathbf{e}$ from basic block encoder
Output: Noised feature $\hat{\mathbf{F}}_\mathbf{n}$ through noise injection
Define: $\hat{\mathbf{F}}_\mathbf{e} \in \mathbb{R}^{B \times H^s \times W^s \times C^s}$, $\mu$ represents the mean and $\sigma$ represents the standard deviation.
$V$ calculates the variance across the batch dimension, * denotes element-wise multiplication.
Prepare
    Calculate the channel-wise mean $\mu \in \mathbb{R}^{B \times C^s}$ by Equation 2.
    Calculate the channel-wise standard deviation $\sigma \in \mathbb{R}^{B \times C^s}$ by Equation 3.
Then
    # Obtain normalized feature
    $\hat{\mathbf{F}}_\mathbf{z} = (\hat{\mathbf{F}}_\mathbf{e} - \mu)/\sigma$
    # Sample tensors from normal distribution
    $\varepsilon_1 \sim N(0,1), \quad \varepsilon_2 \sim N(0,1)$
    # Inject noise with deterministic function
    Noised $\mu \rightarrow \ \mu^\mathbf{n} = \mu + \varepsilon_1 * V(\mu)$
    Noised $\sigma \rightarrow \ \sigma^\mathbf{n} = \sigma + \varepsilon_2 * V(\sigma)$
    # Alter the normalized feature
    $\hat{\mathbf{F}}_\mathbf{n} = \hat{\mathbf{F}}_\mathbf{z} * \sigma^\mathbf{n} + \mu^\mathbf{n}$
Return Noised feature $\hat{\mathbf{F}}_\mathbf{n}$
```

1. **Independence**: ✓, f_i is independent, with each f_i generated from x_i following a different noise distribution.
2. **Existence of Expectation and Variance**: ✓, the expectation μ_i and variance σ_i^2 of f_i exist, as we have calculated the feature statistics before.
3. **Normalization Condition**: ✓, $\sum_{i=1}^n \sigma_i^2 \to \infty$, the number n of training sample is very large.
4. **Lindeberg Condition**: ✓, for any $\varepsilon > 0$,

$$\frac{1}{\sum_{i=1}^n \sigma_i^2} \sum_{i=1}^n E\left[(f_i - \mu_i)^2 \cdot I(|f_i - \mu_i| \geq \varepsilon \sqrt{\sum_{i=1}^n \sigma_i^2}) \right] \to 0$$

Backward: During model training, we only accept input images x_i^α with Gaussian noise at a level of 15, with the feature map represented as f_i^α. As we have proven above, a large number of f_i from different noise distribution can form a normal distribution. Thus, in return, we sample random noise tensors ε_1 and ε_2 from a normal distribution $N(0,\,1)$, and inject them into the feature statistics (μ_i^α and σ_i^α) of feature map f_i^α.

1. Through a proper nonlinear mapping function, we can map the noised f_i^α by ε_1 and ε_2 to match the unseen f_i, for improved generalization capability.
2. We use reparameterization to make this noise injection differentiable, which enables the neural network to automatically learn suitable nonlinear mapping functions for $f_i^\alpha \to f_i$.

A.4 LIMITATION AND FUTURE DIRECTION

While our method has achieved promising results, enhancing both efficiency and overall performance, there are still areas that warrant further exploration. Compared to MT (Chen et al., 2023), our approach generally performs better in most scenarios with 10 times faster inference speeds, particularly in handling mixture noise which is more complex and representative in real cases. However, MT (Chen et al., 2023) exhibits competitive performance under super high-intensity noise conditions due to its stronger smoothing capabilities. Although such high levels of noise (somewhat rare and peculiar) are unlikely to be encountered in real-world conditions, where noise is typically not as artificially extreme as in MT's setting (*i.e.* poisson noise multiplied by the scale factor 2/2.5/3), it is still valuable to investigate how our method can further adapt to super-high noise intensities. Specifically, improving our method's ability to provide stronger smoothing under extremely high noise conditions without excessively smoothing images in moderate noise scenarios remains an important area for future research.

A.5 SUPPLEMENTARY FOR REBUTTALS

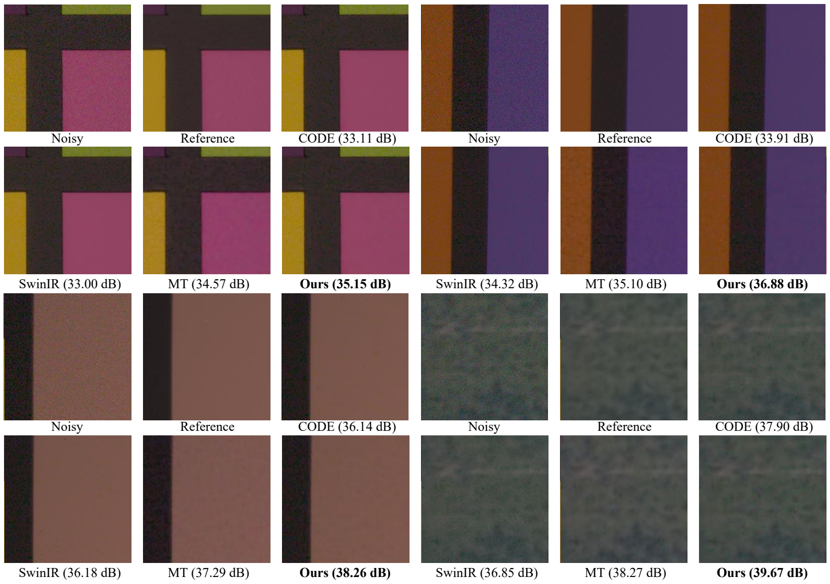

Noisy | Reference | CODE (33.11 dB) | Noisy | Reference | CODE (33.91 dB)

SwinIR (33.00 dB) | MT (34.57 dB) | **Ours (35.15 dB)** | SwinIR (34.32 dB) | MT (35.10 dB) | **Ours (36.88 dB)**

Noisy | Reference | CODE (36.14 dB) | Noisy | Reference | CODE (37.90 dB)

SwinIR (36.18 dB) | MT (37.29 dB) | **Ours (38.26 dB)** | SwinIR (36.85 dB) | MT (38.27 dB) | **Ours (39.67 dB)**

Figure 10: **Supplementary for Rebuttals**. Updated Figure 8 with additional showcases and updated PSNR values for improved clarity and comparison.

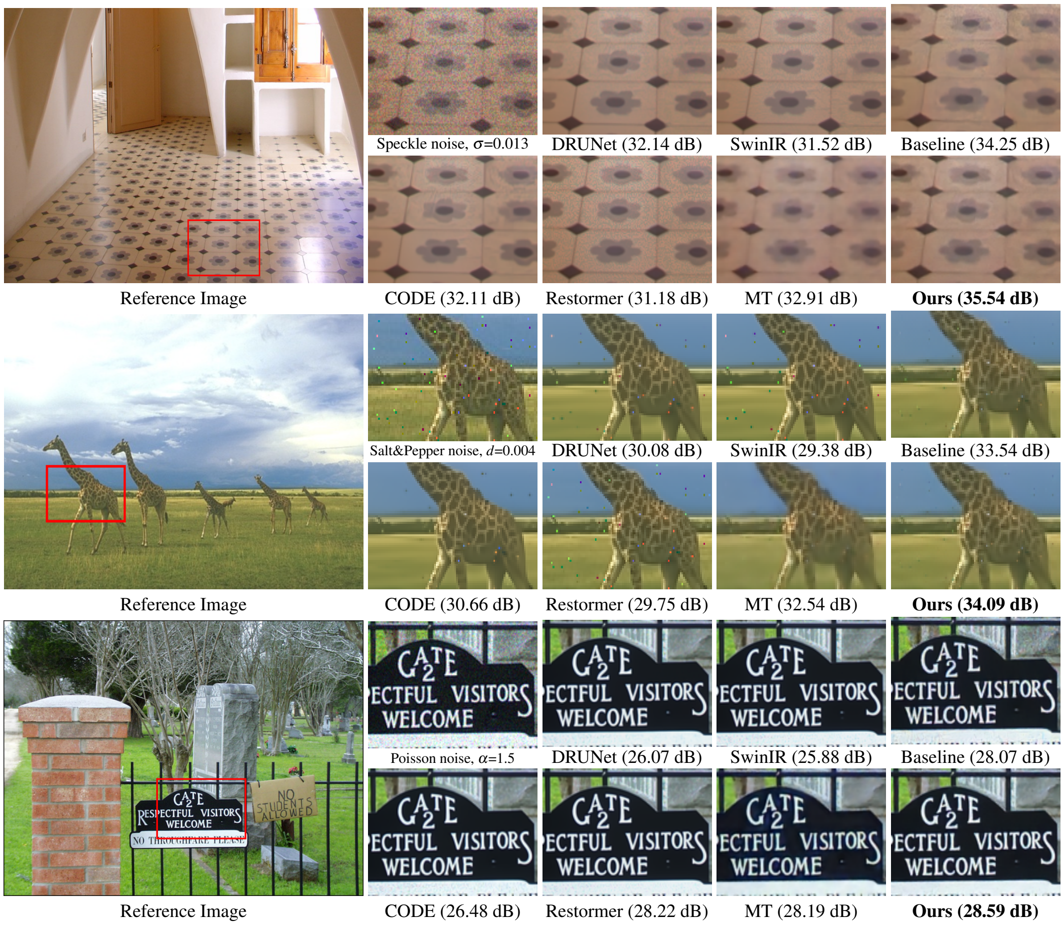

Speckle noise, σ=0.013 | DRUNet (32.14 dB) | SwinIR (31.52 dB) | Baseline (34.25 dB)

Reference Image | CODE (32.11 dB) | Restormer (31.18 dB) | MT (32.91 dB) | **Ours (35.54 dB)**

Salt&Pepper noise, d=0.004 | DRUNet (30.08 dB) | SwinIR (29.38 dB) | Baseline (33.54 dB)

Reference Image | CODE (30.66 dB) | Restormer (29.75 dB) | MT (32.54 dB) | **Ours (34.09 dB)**

Poisson noise, α=1.5 | DRUNet (26.07 dB) | SwinIR (25.88 dB) | Baseline (28.07 dB)

Reference Image | CODE (26.48 dB) | Restormer (28.22 dB) | MT (28.19 dB) | **Ours (28.59 dB)**

Figure 11: **Supplementary for Rebuttals**. Updated Figure 5 with additional PSNR values for improved clarity and comparison.

Dataset	PolyU Xu et al. (2018)		Nam (CC) Nam et al. (2016)	
	PSNR↑	SSIM↑	PSNR↑	SSIM↑
ZS-Denoiser (ZS-N2N) Kim et al. (2024)	31.47	0.8750	34.47	0.9020
ZS-Denoiser (Nbr2Nbr) Kim et al. (2024)	32.93	0.9110	35.39	0.9230
MT Chen et al. (2023)	33.96	0.9260	33.20	0.9209
RNINet (Ours)	**37.59**	**0.9551**	**37.15**	**0.9525**

Table 7: **Supplementary for Rebuttals**. Additional results on PolyU Xu et al. (2018) and Nam Nam et al. (2016) datasets, compared with MT and two zero-shot denoisers introduced in LAN Kim et al. (2024).

Speckle Noise	$\sigma^2 = 0.02$		$\sigma^2 = 0.024$		$\sigma^2 = 0.03$		$\sigma^2 = 0.04$	
Method	PSNR↑	SSIM↑	PSNR↑	SSIM↑	PSNR↑	SSIM↑	PSNR↑	SSIM↑
RNINet-g2p	31.42	0.8425	30.39	0.8153	29.09	0.7801	27.48	0.7341
RNINet-original	32.20	0.8674	31.29	0.8443	30.04	0.8097	28.35	0.7639
Salt & Pepper	$d = 0.002$		$d = 0.004$		$d = 0.008$		$d = 0.012$	
Method	PSNR↑	SSIM↑	PSNR↑	SSIM↑	PSNR↑	SSIM↑	PSNR↑	SSIM↑
RNINet-g2p	34.54	0.9290	32.93	0.9042	30.65	0.8554	29.00	0.8075
RNINet-original	33.91	0.8992	33.04	0.8824	31.50	0.8486	30.11	0.8123
Poisson Noise	$\alpha = 1.5$		$\alpha = 2$		$\alpha = 2.5$		$\alpha = 3$	
Method	PSNR↑	SSIM↑	PSNR↑	SSIM↑	PSNR↑	SSIM↑	PSNR↑	SSIM↑
RNINet-g2p	32.72	0.8747	29.36	0.7658	26.80	0.6730	24.81	0.5970
RNINet-original	33.65	0.9067	31.01	0.8337	28.19	0.7457	25.87	0.6673
Mixture Noise	Level 1		Level 2		Level 3		Level 4	
Method	PSNR↑	SSIM↑	PSNR↑	SSIM↑	PSNR↑	SSIM↑	PSNR↑	SSIM↑
RNINet-g2p	32.79	0.8960	32.51	0.8880	31.24	0.8551	30.22	0.8227
RNINet-original	33.23	0.8956	33.09	0.8935	32.34	0.8774	31.56	0.8575
	Synthetic ISP Noise		Monte Carlo Rendering Noise					
Method	PSNR↑	SSIM↑	PSNR↑ (256 pp)	SSIM↑ (256 pp)	PSNR↑ (128 pp)	SSIM↑ (128 pp)	PSNR↑ (64 pp)	SSIM↑ (64 pp)
RNINet-g2p	30.88	0.7963	31.74	0.8240	29.18	0.7477	26.47	0.6668
RNINet-original	31.15	0.8195	33.36	0.8760	30.34	0.8056	27.38	0.7244

Table 8: **Supplementary for Rebuttals**. Additional comparisons are provided by training our RNINet model on Gaussian noise first, followed by training on Poisson noise. This approach is referred to as RNINet-g2p. The total number of iterations for RNINet-g2p was kept identical to the iterations used for training RNINet exclusively on Gaussian noise (referred to as RNINet-original).

Speckle Noise	$\sigma^2 = 0.02$		$\sigma^2 = 0.024$		$\sigma^2 = 0.03$		$\sigma^2 = 0.04$	
Method	PSNR↑	SSIM↑	PSNR↑	SSIM↑	PSNR↑	SSIM↑	PSNR↑	SSIM↑
DRUNet	29.85	0.8085	28.47	0.7795	26.84	0.7437	24.89	0.6996
SwinIR	29.19	0.7948	27.84	0.7662	26.30	0.7323	24.46	0.6912
Restormer	28.90	0.8008	27.97	0.7794	26.81	0.7522	25.30	0.7174
CODE	29.93	0.7641	28.63	0.7357	27.07	0.7009	25.18	0.6583
baseline	31.57	0.8486	30.66	0.8243	29.50	0.7907	27.93	0.7489
MT	30.48	0.8094	30.20	0.7985	29.69	0.7776	28.66	0.7360
Ours	**32.20**	**0.8674**	**31.29**	**0.8443**	**30.04**	**0.8097**	**28.35**	**0.7639**
Salt & Pepper	$d = 0.002$		$d = 0.004$		$d = 0.008$		$d = 0.012$	
Method	PSNR↑	SSIM↑	PSNR↑	SSIM↑	PSNR↑	SSIM↑	PSNR↑	SSIM↑
DRUNet	32.33	0.8953	30.15	0.8637	27.47	0.8044	25.77	0.7508
SwinIR	31.75	0.8964	29.49	0.8642	26.75	0.8012	25.00	0.7420
Restormer	32.89	0.9246	30.18	0.8828	27.10	0.8088	25.31	0.7459
CODE	32.50	0.8555	30.42	0.8277	27.58	0.7718	25.74	0.7188
baseline	33.53	0.8893	32.69	0.8735	31.19	0.8398	29.83	0.8026
MT	30.88	0.8197	30.76	0.8164	30.46	0.8081	30.09	0.7973
Ours	**33.91**	**0.8992**	**33.04**	**0.8824**	**31.50**	**0.8486**	**30.11**	**0.8123**
Poisson Noise	$\alpha = 1.5$		$\alpha = 2$		$\alpha = 2.5$		$\alpha = 3$	
Method	PSNR↑	SSIM↑	PSNR↑	SSIM↑	PSNR↑	SSIM↑	PSNR↑	SSIM↑
DRUNet	33.24	0.8773	28.26	0.7527	24.74	0.6510	22.27	0.5735
SwinIR	33.04	0.8697	27.84	0.7418	24.48	0.6453	22.13	0.5712
Restormer	31.99	0.8601	28.73	0.7768	25.78	0.693	23.63	0.6312
CODE	32.98	0.8247	28.26	0.7029	24.88	0.6094	22.52	0.5389
baseline	33.36	0.8949	30.44	0.8139	27.79	0.7324	25.60	0.6593
MT	30.76	0.8187	30.10	0.7972	28.56	0.7306	26.70	0.6514
Ours	**33.65**	**0.9067**	**31.01**	**0.8337**	**28.19**	**0.7457**	**25.87**	**0.6673**
Mixture Noise	Level 1		Level 2		Level 3		Level 4	
Method	PSNR↑	SSIM↑	PSNR↑	SSIM↑	PSNR↑	SSIM↑	PSNR↑	SSIM↑
DRUNet	31.73	0.8865	31.48	0.8781	29.91	0.8412	28.60	0.8042
SwinIR	31.32	0.8856	31.05	0.8745	29.40	0.8326	28.07	0.7933
Restormer	31.06	0.8705	30.73	0.8612	29.38	0.8314	28.22	0.8001
CODE	31.65	0.8372	31.36	0.8276	29.75	0.7902	28.43	0.7543
baseline	32.96	0.8887	32.79	0.8851	31.97	0.8651	31.15	0.8419
MT	30.74	0.8176	30.70	0.8168	30.54	0.8133	30.36	0.8085
Ours	**33.23**	**0.8956**	**33.09**	**0.8935**	**32.34**	**0.8774**	**31.56**	**0.8575**

Table 9: Quantitative comparison on the McMaster (Zhang et al., 2011) dataset. Our RNINet outperforms other state-of-the-art methods in most cases, achieving significantly better performance in handling mixture noises, which are more complicated and representative in real application environments.

Speckle Noise	$\sigma^2 = 0.02$		$\sigma^2 = 0.024$		$\sigma^2 = 0.03$		$\sigma^2 = 0.04$	
Method	PSNR↑	SSIM↑	PSNR↑	SSIM↑	PSNR↑	SSIM↑	PSNR↑	SSIM↑
DRUNet	29.31	0.8204	27.97	0.7868	26.34	0.7446	24.35	0.6876
SwinIR	28.88	0.8099	27.54	0.7772	25.98	0.7363	24.07	0.6810
Restormer	29.15	0.8276	28.12	0.8010	26.84	0.7667	25.17	0.7200
CODE	29.36	0.8150	28.06	0.7844	26.49	0.7451	24.56	0.6901
baseline	30.43	0.8567	29.63	0.8326	28.55	0.8005	27.05	0.7538
MT	29.90	0.8752	29.57	0.8678	28.99	0.8511	27.94	0.8144
Ours	**31.21**	**0.8796**	**30.36**	**0.8574**	**29.17**	**0.8233**	**27.54**	**0.7742**
Salt & Pepper	$d = 0.002$		$d = 0.004$		$d = 0.008$		$d = 0.012$	
Method	PSNR↑	SSIM↑	PSNR↑	SSIM↑	PSNR↑	SSIM↑	PSNR↑	SSIM↑
DRUNet	32.6	0.9005	30.63	0.8736	28.08	0.8222	26.39	0.7736
SwinIR	31.87	0.9001	29.84	0.8726	27.24	0.8186	25.5	0.7653
Restormer	33.42	0.9475	30.97	0.9105	27.79	0.8409	25.89	0.7789
CODE	33.04	0.9015	31.24	0.8776	28.42	0.8255	26.49	0.773
baseline	33.07	0.8970	32.48	0.8873	31.30	0.8647	30.15	0.8371
MT	31.16	0.8746	31.06	0.8733	30.80	0.8692	30.48	0.8623
Ours	**33.93**	**0.9092**	**33.21**	**0.8984**	**31.88**	**0.8752**	**30.64**	**0.8484**
Poisson Noise	$\alpha = 1.5$		$\alpha = 2$		$\alpha = 2.5$		$\alpha = 3$	
Method	PSNR↑	SSIM↑	PSNR↑	SSIM↑	PSNR↑	SSIM↑	PSNR↑	SSIM↑
DRUNet	32.25	0.8891	27.44	0.7500	23.84	0.6098	21.30	0.4997
SwinIR	32.15	0.8855	27.14	0.7397	23.69	0.6046	21.28	0.4988
Restormer	32.19	0.8917	28.70	0.7983	25.67	0.6949	23.52	0.6168
CODE	32.34	0.8796	27.47	0.7409	24.03	0.6091	21.67	0.5056
baseline	32.12	0.9025	29.34	0.8203	26.70	0.7183	24.48	0.6255
MT	30.55	0.8842	29.55	0.8696	27.79	0.8053	25.86	0.7171
Ours	**32.69**	**0.9132**	**30.00**	**0.8452**	**27.10**	**0.7387**	**24.77**	**0.6384**
Mixture Noise	Level 1		Level 2		Level 3		Level 4	
Method	PSNR↑	SSIM↑	PSNR↑	SSIM↑	PSNR↑	SSIM↑	PSNR↑	SSIM↑
DRUNet	31.41	0.8946	31.19	0.8885	29.73	0.8568	28.50	0.8235
SwinIR	31.00	0.8935	30.79	0.8864	29.29	0.8523	28.06	0.8177
Restormer	31.08	0.8941	30.83	0.8869	29.52	0.8594	28.40	0.8298
CODE	31.73	0.8902	31.45	0.8824	29.85	0.8460	28.53	0.8089
baseline	32.06	0.8997	31.88	0.8974	31.17	0.8804	30.41	0.8596
MT	30.50	0.8797	30.40	0.8797	30.16	0.8782	29.91	0.8754
Ours	**32.62**	**0.9070**	**32.45**	**0.9058**	**31.73**	**0.8930**	**30.99**	**0.8766**

Table 10: Quantitative comparison on the CBSD68 (Martin et al., 2001) dataset. Our RNINet outperforms other state-of-the-art methods in most cases, achieving significantly better performance in handling mixture noises, which are more complicated and representative in real application environments.

Speckle Noise	$\sigma^2 = 0.02$		$\sigma^2 = 0.024$		$\sigma^2 = 0.03$		$\sigma^2 = 0.04$	
Method	PSNR↑	SSIM↑	PSNR↑	SSIM↑	PSNR↑	SSIM↑	PSNR↑	SSIM↑
DRUNet	29.90	0.8041	28.43	0.7611	26.65	0.7063	24.49	0.6356
SwinIR	29.39	0.7906	27.92	0.7480	26.22	0.6950	24.17	0.6268
Restormer	29.73	0.8125	28.67	0.7820	27.28	0.7377	25.54	0.6843
CODE	30.06	0.8032	28.60	0.7623	26.86	0.7093	24.76	0.6404
baseline	31.08	0.8451	30.20	0.8170	29.07	0.7780	27.41	0.7200
MT	30.65	0.8737	30.33	0.8665	29.74	0.8484	28.59	0.8027
Ours	**31.85**	**0.8697**	**30.95**	**0.8437**	**29.69**	**0.8033**	**27.90**	**0.7425**
Salt & Pepper	$d = 0.002$		$d = 0.004$		$d = 0.008$		$d = 0.012$	
Method	PSNR↑	SSIM↑	PSNR↑	SSIM↑	PSNR↑	SSIM↑	PSNR↑	SSIM↑
DRUNet	33.11	0.8910	31.13	0.8626	28.57	0.8070	26.86	0.7550
SwinIR	32.26	0.8894	30.14	0.8591	27.50	0.7979	25.73	0.7395
Restormer	33.79	0.9352	31.02	0.8907	27.94	0.8152	26.16	0.7542
CODE	33.61	0.8943	31.80	0.8702	28.89	0.8115	26.88	0.7532
baseline	33.58	0.8837	33.04	0.8749	31.93	0.8541	30.84	0.828
MT	31.71	0.8719	31.63	0.8709	31.42	0.8675	31.15	0.8616
Ours	**34.33**	**0.8978**	**33.70**	**0.8880**	**32.49**	**0.8664**	**31.28**	**0.8406**
Poisson Noise	$\alpha = 1.5$		$\alpha = 2$		$\alpha = 2.5$		$\alpha = 3$	
Method	PSNR↑	SSIM↑	PSNR↑	SSIM↑	PSNR↑	SSIM↑	PSNR↑	SSIM↑
DRUNet	32.95	0.8788	27.53	0.7002	23.71	0.5444	21.09	0.4301
SwinIR	32.77	0.8716	27.21	0.6884	23.58	0.5406	21.09	0.4314
Restormer	32.83	0.8805	29.12	0.7665	25.95	0.6448	23.85	0.5630
CODE	33.08	0.8727	27.61	0.6951	23.93	0.5463	21.48	0.4359
baseline	32.81	0.8952	29.72	0.7881	26.77	0.6645	24.40	0.5578
MT	31.21	0.8817	30.26	0.8636	28.29	0.7800	26.03	0.6678
Ours	**33.34**	**0.9048**	**30.39**	**0.8178**	**27.14**	**0.6831**	**24.66**	**0.5685**
Mixture Noise	Level 1		Level 2		Level 3		Level 4	
Method	PSNR↑	SSIM↑	PSNR↑	SSIM↑	PSNR↑	SSIM↑	PSNR↑	SSIM↑
DRUNet	32.14	0.8877	31.87	0.8816	30.33	0.8459	29.06	0.8083
SwinIR	31.60	0.8855	31.33	0.8776	29.76	0.8396	28.49	0.8001
Restormer	31.67	0.8844	31.38	0.8769	30.01	0.8470	28.88	0.8144
CODE	32.45	0.8848	32.10	0.8753	30.38	0.8343	29.01	0.7930
baseline	32.77	0.8915	32.62	0.8896	31.84	0.8727	31.06	0.8501
MT	31.16	0.8776	31.09	0.8774	30.88	0.8761	30.67	0.8737
Ours	**33.26**	**0.8990**	**33.09**	**0.8976**	**32.37**	**0.8851**	**31.65**	**0.8686**

Table 11: Quantitative comparison on the Kodak24 (Franzen, 1999) dataset. Our RNINet outperforms other state-of-the-art methods in most cases, achieving significantly better performance in handling mixture noises, which are more complicated and representative in real application environments.

Speckle Noise	$\sigma^2 = 0.02$		$\sigma^2 = 0.024$		$\sigma^2 = 0.03$		$\sigma^2 = 0.04$	
Method	PSNR↑	SSIM↑	PSNR↑	SSIM↑	PSNR↑	SSIM↑	PSNR↑	SSIM↑
DRUNet	27.98	0.8036	26.63	0.7723	25.05	0.7339	23.16	0.6837
SwinIR	27.51	0.7931	26.19	0.7627	24.68	0.7256	22.88	0.6772
Restormer	28.21	0.8099	27.17	0.7851	25.86	0.7529	24.17	0.7106
CODE	28.06	0.7965	26.76	0.7674	25.26	0.7306	23.45	0.6825
baseline	29.52	0.8475	28.61	0.8227	27.51	0.7905	26.01	0.7464
MT	28.60	0.8831	28.25	0.8706	27.65	0.8466	26.64	0.8043
Ours	**30.16**	**0.8696**	**29.25**	**0.8451**	**28.06**	**0.8113**	**26.48**	**0.7649**
Salt & Pepper	$d = 0.002$		$d = 0.004$		$d = 0.008$		$d = 0.012$	
Method	PSNR↑	SSIM↑	PSNR↑	SSIM↑	PSNR↑	SSIM↑	PSNR↑	SSIM↑
DRUNet	32.40	0.9199	30.47	0.8966	27.93	0.8509	26.25	0.8080
SwinIR	31.49	0.9171	29.43	0.8913	26.85	0.8405	25.16	0.7924
Restormer	32.80	0.938	30.25	0.9054	27.34	0.8481	25.63	0.7994
CODE	32.88	0.9154	31.08	0.8941	28.35	0.8484	26.49	0.8037
baseline	33.08	0.9137	32.35	0.9029	31.01	0.8791	29.80	0.8522
MT	29.75	0.8953	29.64	0.8932	29.38	0.8875	29.09	0.8802
Ours	**33.48**	**0.9215**	**32.70**	**0.9102**	**31.32**	**0.8864**	**30.08**	**0.8606**
Poisson Noise	$\alpha = 1.5$		$\alpha = 2$		$\alpha = 2.5$		$\alpha = 3$	
Method	PSNR↑	SSIM↑	PSNR↑	SSIM↑	PSNR↑	SSIM↑	PSNR↑	SSIM↑
DRUNet	31.97	0.8872	26.93	0.7554	23.44	0.6442	21.02	0.5580
SwinIR	31.85	0.8815	26.60	0.7455	23.27	0.6390	20.96	0.5574
Restormer	31.94	0.8860	28.39	0.7970	25.33	0.7047	22.89	0.6269
CODE	31.98	0.8729	27.01	0.7452	23.69	0.6416	21.42	0.5619
baseline	31.91	0.9098	28.90	0.8231	26.33	0.7355	24.23	0.6600
MT	29.23	0.8961	28.39	0.8768	26.95	0.8144	25.33	0.7365
Ours	**32.18**	**0.9218**	**29.50**	**0.8484**	**26.76**	**0.7537**	**24.57**	**0.6728**
Mixture Noise	Level 1		Level 2		Level 3		Level 4	
Method	PSNR↑	SSIM↑	PSNR↑	SSIM↑	PSNR↑	SSIM↑	PSNR↑	SSIM↑
DRUNet	31.36	0.9091	31.02	0.8977	29.39	0.8600	28.04	0.8239
SwinIR	30.85	0.9035	30.51	0.8909	28.84	0.8508	27.50	0.8141
Restormer	30.91	0.8953	30.62	0.8865	29.20	0.8562	28.07	0.8275
CODE	31.61	0.8961	31.19	0.8830	29.47	0.8432	28.08	0.8067
baseline	31.91	0.9120	31.67	0.9075	30.76	0.8852	29.89	0.8610
MT	29.23	0.8947	29.14	0.8942	28.91	0.8914	28.68	0.8874
Ours	**32.11**	**0.9169**	**31.90**	**0.9146**	**31.10**	**0.8995**	**30.30**	**0.8799**

Table 12: Quantitative comparison on the Urban100 (Huang et al., 2015) dataset. Our RNINet outperforms other state-of-the-art methods in most cases, achieving significantly better performance in handling mixture noises, which are more complicated and representative in real application environments.